ISSN: 0974-5823 Vol. 7 No. 5 May, 2022

*International Journal of Mechanical Engineering*

# Alloyed monolayers of $WX_2$ of Al and Pt wires in Crystallographic phase: A DFT study

**Kumar Saurabh Yadav[1*],**

[1]Department of Physics, Bundelkhand University, Jhansi (U.P)-284128 India

**Ankit Kumar Srivastava[2],**

[2]Department of Physics, Indrashil University, Mehsana 382740, India

**Bhagirath Singh Bhadoria[1]**

[1]Department of Physics, Bundelkhand University, Jhansi (U.P)-284128 India

**Swasti Saxena[3]**

[3]Department of Physics, Sardar Vallabhbhai National Institute of Technology, Surat 395007, India

**ABSTRACT**

We present density functional theory (DFT) based comprehensive study of two-dimensional (2D) alloyed monolayers of noble metals in hexagonal-phase within numerical atomic orbitals and plane wave basis sets methods. Positive phonon frequencies in the monolayers studied indicate that the metals are dynamically stable. The alloyed monolayers containing Pt show higher structural stability (binding energy and tensile strength) and exhibit metallic and ferromagnetic properties among the alloyed monolayers. Intriguingly, alloying monolayers with Al results in semiconducting behaviour, whereas alloyed $WX_2$ monolayers exhibit Dirac-cone-like properties at high symmetry points, in dielectric spectra for all of the structures investigated show anisotropic behaviour. For Pt-containing alloyed monolayers, tunnelling characteristics suggest an NDR zone. The considered alloyed monolayers may potentially be useful as building-blocks for the applications in nano and optoelectronics.

**Keyword:** Atomic wires, DFT, Alloyed Monolayers, Band structure, Mechanical properties, $WX_2$.

## 1. Introduction:

Researchers have examined graphene, a two-dimensional (2D) honeycomb structure of carbon, in great detail [1–4], but it lacks a band gap. Many key applications in optics and transistor technology, however, need a band gap, prompting intense research efforts to functionalize it and manipulate the band gap. Layered transition metal dichalcogenides (LTMDCs), such as $WS_2$, have recently emerged as competitive materials for nanoelectronics due to unique features such as the presence of a band gap, temperature stability up to 1100 $^0$C, and the lack of dangling bonds. The result was the successful development of a monolayer $WS_2$-based field effect transistor recently. This has piqued people's curiosity in learning more about the unique features of different LTMDC monolayers.

Although several features of bulk LTDMCs have been examined before [6–12], it is only lately [13-14] that quantum confinement has been discovered to have a significant influence in the electrical and dielectric properties of multilayer TMDCs. A common example of a layered transition metal dichalcogenide family of materials is $WX_2$ (X = S, Se, Te). $WX_2$ bulk crystals have a hexagonal shape with space group P63/mmc, which corresponds to space group 194. They're built up with X-M-X (M=Mo, W) units that are stacked van der Walls-bonded. A $MX_2$ monolayer is made up of two hexagonal planes of chalchogen (X) atoms and an intermediate hexagonal plane of transition metal (M) atoms that are coordinated by ionic-covalent interactions, with the X atoms arranged in a trigonal prismatic pattern as illustrated in Figure 1.

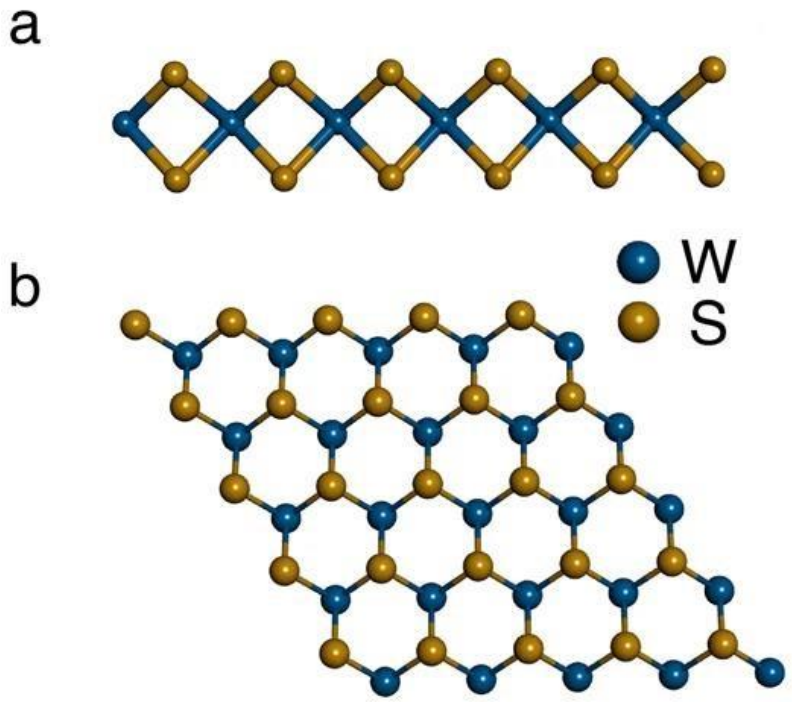


Figure 1: (a) Side view of $WS_2$ (b) Top View of $WS_2$

Novoselov et al. [15] developed a cleavage approach. They were able to obtain 6.5 Å thick honeycomb monolayers. Coleman et al. [16] also demonstrated that layered materials such $MoS_2$, $MoSe_2$, $MoTe_2$, $WS_2$, $TaSe_2$, $NbSe_2$, $NiTe_2$, BN, and $Te_2$ may be exfoliated effectively into individual layers. Because of their ease of shearing, these materials are being used in lubricating applications [17]. Photocatalysis, optoelectronics, and photovoltaics are among the other uses of TMDCs that have been researched [18–22]. Optical spectroscopy has recently been used to investigate atomically thin $MoS_2$, revealing it to be a novel direct band gap semiconductor with a band gap of 0.7 eV to 2.0 eV [7–9]. $MX_2$ materials have a wide variety of band gaps, making them good candidates for device applications and maybe a viable alternative for Silicon (Si).

We set out to determine the electronic structure of sulphides, selenides, and tellurides of both Molybdenum (Mo) and Tungsten (W) after being inspired by recent investigations of the different features of monolayer $WS_2$ [23].

The lattice characteristics and electronic structure of monolayer $MX_2$ (M = Mo, W; S = S, Se, Te) described as 1H-$MX_2$ are reported in this study. Except for $WTe_2$, which has distorted octahedral coordination, all of the materials tested exhibit hexagonal symmetry (1H) with trigonal prismatic structure as shown in Figures 1 and 2, although we have only utilised hexagonal symmetry (1H) for direct comparison. By methodically lowering the thickness of materials from bulk to monolayer, we show how quantum confinement affects the electrical structure of distinct LTMDCs. The VASP technique was used to execute density functional theory (DFT) computations utilising ab-initio pseudopotential and numerical atomic orbitals (NAO's) basis sets inside the local density approximation (LDA). The prior electronic structure calculations only applied to bulk systems and the monolayer $WX_2$, however the results for the monolayers provided in this research are published.

Metal nanostructures' characteristics are known to be directly linked to their crystal structure.In bulk, noble metals have a variety of crystal forms; for example, Ag has two polymorphs, 9R-[24] and 4H-polytype [25]. Previous investigations [32-33] have shown the existence of hexagonal phase in one-dimensional (1D) hetero-nanostructures [26], thin films [26], nanorods [28– 31], and nano wires of Silver. Marshall et al.[34] recently described a crystallisation route for the meta stable HCP phase in gold. Gold has also been synthesised in several nanostructures with HCP structure in the recent decade, including nanoparticles [35], nanowires [37], nanobelts or nanoribbons [38], nanoplates [6], nanosheets [39], and nanotubes [40]. The presence of gold nanoparticles in HCP frameworks makes understanding their characteristics intriguing from both a basic and technological standpoint.

Noble metal nanoplates and nanosheets have a wide range of uses, but their utilisation is limited due to limited reserves and expensive prices. Noble metals have been alloyed with earth plentiful metals to improve their qualities at a low cost [41]. The use of alloyed nanomaterials in which d-band vacancies of a Group 10 (Pt) metal are gradually filled by a Group 13 (Al) metal has piqued attention in the field of electronics [42–45]. It's worth noting that heterogeneous Al-Pt nanostructures with far superior characteristics than their pristine counterparts have been created for use in optics, electronics, protective coatings, bio-sensing, drug delivery, and catalysis [44–45]. Despite the fact that hexagonal structure is not an apparent choice for noble metal alloyed sheets, the above-mentioned recent findings have prompted it.

So far, quasi-1D batches of $WX_2$-wires have been commonly generated in bulk inorganic synthesis by stabilising these atomic wires with different counter ions (such as alkali metals or iodine) [46-47] aligned and evenly spaced arrays of Pt and Al wires on Alloyed monomers, [49] free bundles of Pt and Al wires without counterions, Inside single-wall carbon nanotubes, $WS_2$ and $WSe_2$ wires were recently synthesised [50]. Individual $MX_2$ (M = W; X = S, Se), $WSe_2$, and $WS_2$ alloy wires were also created by shaping their monolayer equivalents [48]. These atomic wires have self-adaptive connections to the monolayers and can withstand extreme mechanical deformation while remaining conductive. Individual wire twisting, axial kinking, and branching, as well as wellordered junction structures that join numerous atomic wires such as Pt and Al, have all been accomplished. Many types of subnanometer-width atomic wires are now possible because to developing manufacturing processes.

On the theoretical side, much work has gone into understanding the electrical, transport, and mechanical characteristics of metallic TMC wires, as well as investigating the implications of intercalation and heteroatom doping on their physical properties, particularly the likelihood of band gap formation opening [51]. Despite the aforementioned results, all prior experimental and theoretical investigations on metallic wires on molybdenum chalcogenides and tungsten chalcogenides as sandwich structures only concentrated on a few types of metallic wires. Because various 2D TMDs with a variety of structural phases and characteristics have been produced in the lab, [52] it's logical to wonder if additional transition metal elements besides Al and Pt may create stable 1D chalcogenide wires.

If that's the case, what would their geometrical structures be?

How do they compare to $WX_2$-Al monolayers and $WX_2$-Pt monolayers with atomic wires (Al and Pt), as well as their 2D TMD equivalents, in terms of electrical and mechanical properties?

Is it feasible to create 1D TMC wires with customised band topologies for a certain device?

To answer these exciting problems, we investigate atomic wires of transition metal chalcogenides in the stoichiometry of $MX_2$ (X = S, Se, Te; M = 3d, 4d, and 5d elements) for the first time. The electrical architectures of several types of wires are explored in order to screen 1D semiconductors and ferromagnets, respectively, for carrier mobility and Curie temperature. We go on to look into the mechanical characteristics of atomic wires, explicate the management of ferromagnetic exchange strength strain engineering, and offer a number of 1D flexible ferromagnetism with high Curie temperatures for spintronics.

## 2. Computational Methods

The Vienna Ab-initio Simulation Package (VASP) [53] was used to execute the computational computations for DFT-based first principle methods, employing the plane wave basis set with an energy cutoff of 500 eV and the projector augmented wave (PAW) [54] potentials to characterise the electron–ion interactions. For the exchange-correlation functional [56], Perdew, Burke, and Ernzerhof (PBE) parametrized the generalised gradient approximation (GGA) [55]. To minimise contact between the atomic wire and its duplicate, the unit cells of Al and Pt wires were periodic along the z axis and a vacuum space of 20 was added in the other two directions. A 1 x 1 x 8, k-point grid based on the Monkhorst–Pack technique [57] was used to sample the Brillouin zone. With converging requirements of $10^{-6}$ eV for energy and 0.005 $eV^{-1}$ for force, all 1D structures were thoroughly optimised for both ionic and cell degrees of freedom. The supercell approach was then used to calculate the phonon dispersions of all metal wires. We also estimated the electronic band structures of the semiconducting wires because the PBE functional is known to underestimate the band gap of a semiconductor.

## 3. Results and Discussion

### 3.1. Structure and Stability of 1D $WX_2$-Atomic Wires

The atomic structures of $WX_2$ (X = S, Se, Te) wires, which were synthesised in the lab, are shown in Figures 1a and 1b. We created monolayers for the other 3d, 4d, and 5d transition metal chalcogenide wires based on existing metal wires. Because Al is a P-block element with a greater atomic size, traditional DFT approaches may be unable to accurately anticipate the geometrical and electrical architectures of Al atomic wires. Figures 1a and 1b show the optimal structures of all TMC atomic wires investigated. Metallic wires

made consisting of group III and VIII elements are generally strong conductors, however their 1D metallic wires have noticeable deformations and reduced symmetry. This is due to the group III and VIII transition metal atoms having fewer d electrons and a greater atomic radius. The M–M bonds are somewhat weak after contributing electrons to the S atoms; hence, structural deformation from the symmetric octahedral backbone can assist increase the M–S and M–M interactions.

Sulfide, selenide, and telluride monolayers with $WX_2$ monolayers have comparable structures for a given transition metal element M, with the M–X bond length rising as X moves from S to Se to Te. This paper presents thorough geometrical characteristics and bond overlap population study of several TMC atomic wires.

Table 1. Binding Energies ($E_b$), Formation Energies ($E_{form}$), and Optimized Lattice Constants ($c$) of alloyed-Atomic Wires

| | $E_b$ (eV) | | | $E_{form}$ (eV) | | | $c$ (Å) | | |
|---|---|---|---|---|---|---|---|---|---|
| | **S** | **Se** | **Te** | **S** | **Se** | **Te** | **S** | **Se** | **Te** |
| **Mo** | 5.92 | 5.57 | 5.25 | 0.52 | 0.43 | 0.22 | 4.36 | 4.45 | 4.59 |
| **W** | 6.11 | 5.77 | 5.44 | 0.33 | 0.25 | 0.03 | 4.37 | 4.46 | 4.57 |
| **Mn** | 4.09 | 3.71 | 3.34 | –0.24 | –0.36 | –0.61 | 4.10 | 4.22 | 4.33 |
| **Fe** | 4.65 | 4.29 | | 0.35 | 0.26 | | 4.07 | 4.19 | |
| **Co** | 4.73 | 4.40 | 4.15 | 0.27 | 0.20 | 0.05 | 4.00 | 4.16 | 4.26 |
| **Ni** | 4.42 | 4.10 | 3.87 | 0.31 | 0.25 | 0.13 | 4.08 | 4.23 | 4.40 |
| **Pt** | **4.44** | **4.24** | **4.17** | **0.03** | **0.09** | **0.13** | **4.50** | **4.65** | **4.84** |

To characterise the dynamic stability of all the atomic wires, the phonon dispersions were estimated. In the whole phonon spectrum, all TMC wires are dynamically stable without imaginary frequency. We also confirmed that these metallic wires may be properly separated, meaning that they interact with one another via vdW interaction.

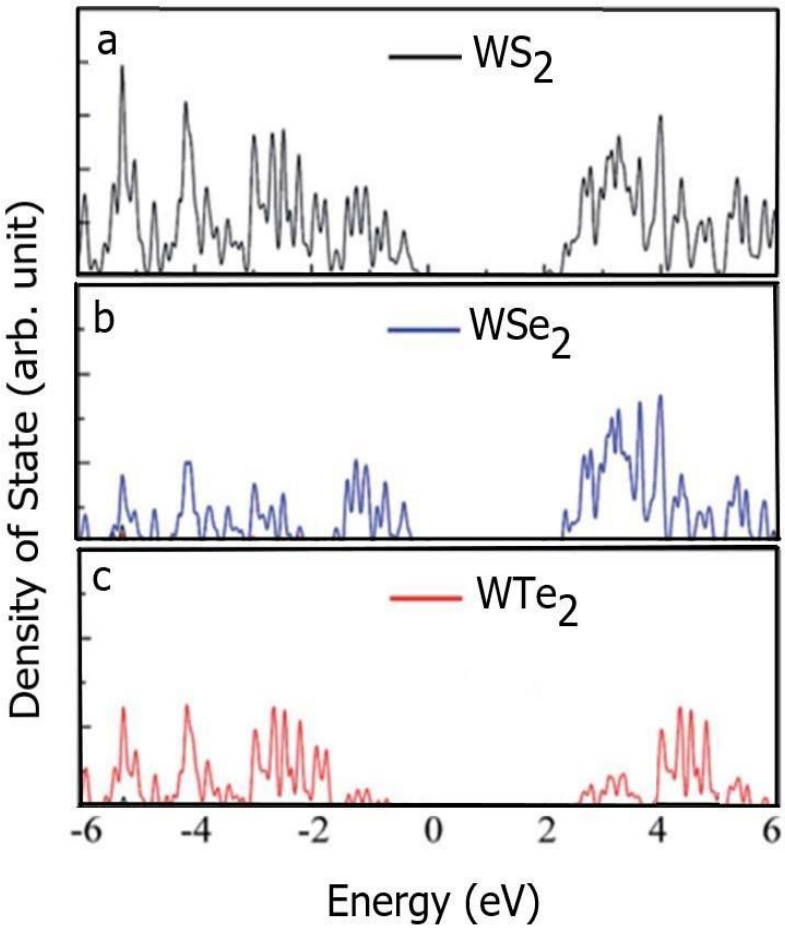


Figure 2: Density of state for (a) $WS_2$ (b) $WSe_2$ (c) $WTe_2$ respectively.

### 3.2. Structural properties

The computed values of the lattice constant, bond length, and binding energies of the examined systems are listed in Table 1. Our earlier research [58] described the structural characteristics of pure noble metal monolayers. The lattice constant values for the alloyed monolayers under investigation. The negative binding energy in each example (Table 1) indicates that all systems are energetically stable. The average binding energies of alloyed systems are higher than those of their pristine counterparts, indicating that alloyed monolayers are more stable than their pristine counterparts and that alloy production is encouraged VASP calculations show that the binding energies follow the Al>Pt trend. It's worth noting that the values derived from two codes varied by around 6% (Table 1).

The Pt-containing alloyed monolayers are energetically more stable than the other alloyed monolayers investigated. All alloyed mono-layers tested were found to be dynamically stable.

### 3.3. Mechanical properties

When a crystal is squeezed or stretched from its equilibrium state, strain plays a vital role. It has the potential to alter device performance and can be used to improve device applications in NEMS and NOMS (nano electro-mechanical systems) (nano optomechanical systems). The value of ultimate tensile strain is equal to the greatest value of strain at which stress changes directly with strain, and the associated value of stress is equal to the system's ultimate tensile strength. The capacity of a system to bear load is referred to as its tensile strength.

Table 2 compares the values of ultimate tensile strain and strength derived from VASP for all investigated systems. It should be emphasised that the tensile strength of alloyed monolayers is comparable to that of their pure counterparts [58].The tensile strength of Pt-containing systems is lower than pristine Pt monolayers but higher than other component atoms of alloyed monolayers. The maximum tensile strength among the examined systems is $WS_2$-Pt, which varies as $WS_2$-Pt >$WSe_2$Pt >$WS_2$-Al

>$WTe_2$-Pt >$WSe_2$-Al >$WTe_2$-Al. The greater bonding, as shown by the binding energies of the examined systems, is responsible for these developments.

### 3.4. Electronic and magnetic properties

The electronic band structure and related spin polarised total and partial density of states as a function of energy for $WS_2$-Pt, $WS_2$-Al, $WSe_2$-Pt, $WSe_2$-Al, $WTe_2$-Al, and $WTe_2$-Pt monolayers have been displayed in Fig. 2 to better understand the electronic features of alloyed monolayers. The band structures calculated using VASP are found to be comparable. The electronic band structures for several systems under investigation have been estimated along the Brillouinzone's Γ-M-K-Γ direction. All Pt containing alloyed monolayers ($WS_2$-Pt, $WSe_2$-Pt, and $WTe_2$-Pt) are metallic in nature, according to the electronic band structure, and their properties are fairly comparable to the electronic band structure of pure Pt monolayer described in earlier work [58]. Alloyed monolayers containing Al ($WS_2$-Al and $WSe_2$-Al) are semiconducting in nature. For the $WS_2$-Al monolayer, which sits between the M and K high symmetry points of Brillouinzone, an indirect band gap of 0.46 eV has been computed.

At the M high symmetry point, the $WSe_2$-Al monolayer has a direct bandgap of 0.88 eV. The band-gap values calculated by VASP differ by less than 2% [(Table 2) of Supplementary material]. In earlier research [59], alloyed nanowires of these noble metals exhibited a similar behaviour. Two conical intersections (Dirac-cone like behaviour) crossing the Fermi-level are seen in the $WSe_2$-Al monolayer, one from the conduction band at high symmetry point M and the other from the valence band at high symmetry point K. The behaviour of the $WS_2$-Al monolayer is comparable to that of virgin Pt and Al monolayers [58]. In case alloyed monolayers, the values of magnetic moment (b), tensile strength, and tensile strain are shown in Table 2.

| For comparison | $WS_2$-Al | $WSe_2$-Al | $WTe_2$-Al | $WS_2$-Pt | $WSe_2$-Pt | $WTe_2$-Pt |
|---|---|---|---|---|---|---|
| Property | 0.00 | 0.00 | 0.00 | 0.58 | 0.41 | 0.45 |
| Magnetic Moment ($\mu_b$) | (0.0) | (0.0) | (0.0) | (0.57) | (0.36) | (0.51) |
| Tensile strength (GPa) | 1.77 | 1.97 | 1.49 | 2.49 | 1.86 | 2.64 |
| Tensile strain | (1.46) | (2.32) | (1.35) | (2.52) | (1.81) | (2.62) |
| (%) | 16(14) | 16(14) | 16(14) | 14(14) | 16(14) | 20(14) |

We have also calculated the magnetic moment as given in Table 2 (($\mu_b$=$Q_\uparrow$−$Q_\downarrow$), where $Q_\uparrow$ in the Mulliken charge population for the spin up and $Q_\downarrow$ is the Mulliken charge population for the spin down states) Magnetic moments have also been estimated using the VASP algorithm, and the density of state graphs of the investigated systems are identical.

The density of states plots of all Pt containing alloyed monolayers ($WS_2$-Pt, $WSe_2$-Pt, and WTe2-Pt) show that Pt, 5d orbitals around the Fermi-level contribute significantly to the density of states. Al, P orbitals contribute significantly to the density of states at the Fermi level in alloyed monolayers containing Al ($WS_2$-Al and $WSe_2$-Al) [Fig 2]. The density of states maps of the alloyed monolayers containing Pt ($WS_2$-Pt, $WSe_2$-Pt, and $WTe_2$-Pt) reveals that they are magnetic in nature. The magnitudes of the spin up and spin down states differ, with the spin up states contributing significantly, favouring ferromagnetism. The d-orbitals, notably the Pt 5d orbitals, provide a significant contribution to ferromagnetism. All of the other systems investigated are non-magnetic, with both spin up and spin down density of states equal in magnitude, resulting in no net magnetic moment.

**Conclusion:**

This research demonstrates that $WS_2$ nanotubes are both ultra-strong and elastic, setting them apart from other materials. A discrete number of atomistic flaws and the inherent strength of the W–S chemical bond determine the mechanical characteristics of $WS_2$ nanotubes. Individual nanotubes have therefore been proved to have perfect strength, demonstrating that defect-free structures are possible. Nonetheless, these high-strength, ductile materials are suitable for a wide range of applications, from nanocomposites to nanomachines.

In conclusion, we investigated the feasibility of 3d, 4d, and 5d transition metal and chalcogen (S, Se, and Te) elements forming 1D metal wires with well-defined geometrical shapes, inspired by synthetic atomic wires of Tungsten chalcogenides. We found atomic wires with adequate dynamic and thermal stabilities and various electronic band structures using high-throughput DFT simulations,

the majority of which could be manufactured from their bulk transition metal and chalcogen predecessors. Some of them may be air-stable. Our theoretical study suggests a family of 1D $WS_2$-wired materials with a diverse set of physical features.

They might open the door to discovering new states of matter through the quantum size effect and producing nanodevices with atomic accuracy.

In Summary, structural, electrical, magnetic, mechanical, dielectric, vibrational, and transport characteristics of ultra thin alloyed nanostructures were investigated using a comparative density functional theory (DFT)-based comprehensive analysis. Alloyed monolayers have similar lattice constant values to their pure counterparts. The average binding energy of these alloyed structures is higher than that of their pure counterparts, indicating that the alloyed structure is more energetically stable. The binding energy of Pt-containing alloyed monolayers is greater. All of the alloyed monolayers investigated had positive phonon frequencies for all modes at all high symmetry sites, indicating that the systems are dynamically stable. Metallic and ferromagnetic in nature, the Ptcontaining alloyed monolayers have greater tensile strengths. The Al-containing alloyed monolayers have a band gap of 0.46 eV and 0.88 eV, respectively, and are semi-conducting. The infrared area contains the reflectance and absorption edges for alloyed monolayers. The alloyed monolayers under consideration might be beneficial in nanoelectronics, optoelectronics, magnetoelectronics, and spintronics.

**References:**


1. A.K. Geim, K.S. Novoselov, The rise of graphene, Nature Mater. 6, 183 (2007)
2. A.K. Geim, Graphene: Status and Prospects, Science 324, 1530 (2009)
3. C.N.R. Rao, A.K. Sood, K.S. Subrahmanyam, A. Govindraj, Angew. Graphene: the new two-dimensional nanomaterial, Chem. Int. Ed. 48, 7752 (2009)
4. O.V. Sedelnikova, L.G. Bulusheva, A.V. Okotrub, *Ab initio* study of dielectric response of rippled graphene, J.Chem. Phys. 134, 244707 (2011)
5. B. Radisavljevic, A. Radenovic, J. Brivio, V. Giacometti, Single-layer MoS2 transistors A. Kis, Nature Nanotechnol. 6, 147 (2011)
6. J. Wilson, A. Yoffe, The transition metal dichalcogenides discussion and interpretation of the observed optical, electrical and structural properties, Adv. Phys. 18, 193 (1969)
7. A.H. Reshak, S. Auluck, Calculated optical properties of 2H−MoS2 intercalated with lithium, Phys. Rev. B 68, 125101 (2003)
8. A.H. Reshak, S. Auluck, Band structure and optical response of 2H−$MoX_2$ compounds (X=S, Se, and Te) Phys. Rev. B 71, 155114 (2005)
9. A.H. Reshak, S. Auluck, Electronic and optical properties of 2H−$WSe_2$ intercalated with copper, Phys. Rev. B 68, 195107 (2003)
10. A. R. Beal, J.C. Knights, W.Y. Liang, Transmission spectra of some transition metal dichalcogenides. II. Group VIA: trigonal prismatic coordination J. Phys. C Solid State Phys. 5, 3540 (1972)
11. H.P. Hughes, W.Y. Liang, Vacuum ultraviolet reflectivity spectra of the molybdenum and tungsten dichalcogenides, J. Phys. C: Solid State Phys. 7, 1023 (1974)
12. A.R. Beal, H.P. Hughes, Kramers-Kronig analysis of the reflectivity spectra of 2H-$MoS_2$, 2H-$MoSe_2$ and 2H-$MoTe_2$ J. Phys. C: Solid State Phys. 12, 881 (1979)
13. A. Kuc, N. Zibouche, T. Heine, Influence of quantum confinement on the electronic structure of the transition metal sulfide TS2 Phys. Rev. B 83, 245213 (2011)
14. P. Johari, V.B. Shenoy, Tunable Dielectric Properties of Transition Metal Dichalcogenides, ACS Nano 5, 5903 (1979)
15. K. Novoselov, D. Jiang, F. Schedin, T. Booth, V. Khotkevich, S. Morozov, A. Geim, Two-dimensional atomic crystals, Proc. Natl. Acad. Sci. USA 102, 10451, (2005)
16. J.N. Coleman et al., Two-Dimensional Nanosheets Produced by Liquid Exfoliation of Layered Materials, Science 331, 568 (2011)
17. L.F. Matthesis, Energy Bands for 2H−$NbSe_2$ and 2H−$MoS_2$**,** Phys. Rev. Lett. 30, 784 (1973)
18. J. Wilcoxon, T. Thurston, J. Martin, Applications of metal and semiconductor nanoclusters as thermal and photocatalysts, Nanostruct. Mater. 12, 993 (1999)
19. K. Kam, B. Parkinson, Detailed photocurrent spectroscopy of the semiconducting group VIB transition metal dichalcogenides J. Phys. Chem. 86, 463 (1982)

20. R. Coehoorn, C. Hass, R.A. Degroot, Electronic structure of $MoSe_2$, $MoS_2$, and $WSe_2$ II. The nature of the optical band gaps, Phys. Rev. B 35, 6203 (1987)

21. R. Tenne, A. Wold, Passivation of recombination centers in *n*-$WSe_2$ yields high efficiency (>14%) photoelectrochemical cell Appl. Phys. Lett. 47, 707 (1985)

22. W. Sienicki, T. Hryniewicz, Tungsten diselenide heterojunction photoelectrodes Solar Energy Mater. Solar Cells 43, 67 (1996)

23. K. F. Mak, C. Lee, J. Hone, J. Shan, T.F. Heinz, Atomically thin $MoS_2$: a new direct-gap semiconductor, Phys. Rev. Lett. 105, 136805 (2010)

24. F. Ernst, M. W. Finnis, D. Hofmann, T. Muschik, U.Schönberger, U.Wolf, M. Methfessel, Theoretical prediction and direct observation of the 9R structure in Ag, Phys. Rev.Lett. 69(4) (1992)620–623.

25. D. Novgorodova, A.I. Gorshkov, A.V. Mokhov, Native silver and its new structural modifications, Zap. Vses. Mineral. Obshch. 108(1979)552–563.

26. X. S. Shen, G. Z. Wang, X. Hong, X. Xie, W. Zhu, D. P. Li, Anisotropic growth of one-dimensional silver rod–needle and plate–belthetero nano structures induced by twins and hcp phase,J.Am.Chem.Soc.131(31)(2009)10812–10813.

27. P. Taneja, R. Banerjee, P. Ayyub, R. Chandra, G.K. Dey, Observation of a hexagonal (4H) phase in nano crystalline silver, Phys. Rev. B64 (3) (2001) 033405.

28. X.H.Liu, J.Luo, J.Zhu, Size effect on the crystal structure of silver nano wires, NanoLett.6(3) (2006) 408–412.

29. A. Singh, A. Ghosh, Stabilizing high-energy crystal structure in silver nano wires with under potential electro chemistry, J.Phys. Chem. C112 (10) (2008) 3460–3463.

30. B. Wang, G. T. Fei, Y. Zhou, B. Wu, X.Zhu, L.Zhang, Controlled growth and phase transition of silver nano wires with dense length wise twins and stacking faults, Cryst. Growth Des.28 (8) (2008)3073–3076.

31. C. Liang, K. Terabe, T. Hasegawa, M. Aono, Formation of meta stable silver nano-wires of hexagonal structure and their structural transformation under electron beam irradiation, Japn. J. Appl. Phys. 45 (7) (2006) 6046.

32. I. Chakraborty, D. Carvalho, S. N. Shirodkar, S. Lahiri, S. Bhattacharyya, R. Banerjee, U.Waghmare, P.Ayyub, Novel hexagonal poly types of silver: growth,characterization and first-principles calculations, J. Phys.: Condens. Matter 23(2011)1–12325401.

33. I. Chakraborty, S. N.Shirodkar, S.Gohil, U. V. Waghmare, P. Ayyub, Astable, quasi-2D modification of silver:optical, electronic, vibrationaland mechanical properties, and first principles calculations, J. Phys.:Condens. Matter 26 (2014) 1–10025402.

34. A.F. Marshall, S.V. Thombare, P. C. Mc Intyre, Crystallization pathway for meta stable hexagonal close-packed gold in germanium nanowire catalysts, Cryst. Growth Des. 15 (2015) 3734–3739.

35. A. F. Marshall, I. A. Goldthorpe, H. Adhikari, M. Koto,Y.-C. Wang, L. Fu, E.Olsson, P. C. McIntyre, Hexagonal close packed structure of au nano catalysts solidified after Ge nanowire vapor–liquid–solid growth, Nano Lett. 10 (9) (2010) 3302–3306.

36. X. Huang, S. Li, S. Wu,Y. Huang, F.Boey, C. L. Gan, H. Zhang,Graphene oxide-templated synthesis of ultra thin or tadpole-shaped au nanowires with alternating hcp and fcc domains,Adv.Mater.24 (2012) 979–983.

37. C. M. Payne, D.E.T sentalovich, D. N. Benoit, W.Guo, L.J.E. Anderson, V. L. Colvin, M. Pasquali, J. H. Hafner, Synthesis and crystal structure of gold nanobelts, Chem.Mater.26(6) (2014) 1999–2004.

38. Z. Fan, M. Bosman,X.Huang, D. Huang, Y.Yu, K.P.Ong,Y.A. Akimov, L. Wu, B. Li, J. Wu, Y. Huang, Q. Liu, C. E. Png, C. L. Gan, P. Yang, H. Zhang, Stabilization of 4H hexagonal phase in gold nanoribbons, Nat.Commun.6(2015)7684.

39. X. Huang, S. Li, Y. Huang, S. Wu, X. Zhuo, S. Li, C. L. Gan, F. Boey, C. A. Mirkin, H. Zhang, Synthesis of hexagonal close-packed gold nanostructures, Nat.Commun.2 (2011) 292.

40. Y. Oshima, A. Onga, K. Takayanagi, Helical gold nanotube synthesized at 150K, Phys, Rev. Lett.91(20) (2003) 205503-1-205503-4.

41. J. Wu, P.Li,Y.-T.Pan,S.Warren,X.Yin,H.Yang, Surface lattice-engineered bi-metallic nano particles and their catalytic properties, Chem. Soc. Rev. 41 (2012) 8066–8074.

42. X. Teng, M. Feygenson, Q. Wang, J. He, W. Du, A.I .Frenkel, W. Han, M. Aronson, Electronic and magnetic properties of ultra thin Au/Pt nanowires, NanoLett. 9(9) (2009) 3177–3184.

43. M.F. Luo, C.C.Wang, G.R. Hu, W.R. Lin, C.Y. Ho, Y.C. Lin, Y.J. Hsu, Active alloying of Au with Pt in nanoclusters supported on a thin film of $Al_2O_3$/NiAl(1 0 0), J. Phys.Chem.C113(2009)21054–21062.

44. G. Selvarani, S.V. Selvaganesh,S.Krishnamurthy, G. V. M. Kiruthika, P.Sridhar, S. Pitchumani, A. K. Shukla, A methanol-tolerant carbon-supported Pt–Au alloy cathode catalyst for direct methanol fuel cells and itse valuation by DFT, J.Phys.Chem.C113(17) (2009) 7461–7468.

45. R. M. Ormerod, C. J. Baddeley, R. M. Lambert, Activealloying of Au with Pt in nanoclusters supported on a thin film of $Al_2O_3$/NiAl(10 0), Surf. Sci.259 (1–2) (1991)709–713.

46. C.C. Li,W.P. Cai, B.Q.Cao, F.Q. Sun, Y. Li,C.X. Kan, L.D. Zhang, Mass synthesis oflarge single-crystal Au nanosheets based on a polyol process, Adv. Funct. Mater. 16(1)(2006)83–90.

47. N. Krasteva, I. Besnard, B. Guse, R. E. Bauer, K. Mullen, A. Yasuda, T. Vossmeyer, Self-assembled gold nanoparticle/dendrimer composite films for vapor sensing applications, Nano Lett.2 (5)(2002)551–555.

48. S.-J. Hsu, I.J.B. Lin, Synthesis of gold nano sheets through thermolysis of mixtures of long chain 1-alkylimidazole and hydrogen tetra chloroaurate (III), J. Chin. Chem. Soc.56 (1) (2009) 98–106.

49. S. Rodriguez-Barrero, J. Fernandez Larrinoa, I. Azkona, L .N. Lopezde Lacalle, R. Polvorosa, Enhanced performance of nano structured coatings for drilling by droplet elimination, Mater. Manuf. Process. 31(2016)593– 602.

50. J. Kim,Y. Lee, S.Sun, Structurally ordered FePt nanoparticles and their enhanced catalysis for oxygen reduction reaction, J.Am. Chem.Soc.132 (14) (2010)4996–4997.

51. X. S. Shen, G. Z. Wang, X. Hong, X. Xie, W. Zhu, D. P. Li, Anisotropic growth of one-dimensional silver rod–needle and plate–belthetero nano structures induced by twins and hcp phase,J.Am.Chem.Soc.131(31)(2009)10812–10813.

52. P. Taneja, R. Banerjee, P. Ayyub, R. Chandra, G.K. Dey, Observation of a hexagonal (4H) phase in nano crystalline silver, Phys. Rev. B64 (3) (2001) 033405.

53. X.H.Liu, J.Luo, J.Zhu, Size effect on the crystal structure of silver nano wires, NanoLett.6(3) (2006) 408–412.

54. B. Wang, G. T. Fei, Y. Zhou, B. Wu, X.Zhu, L.Zhang, Controlled growth and phase transition of silver nano wires with dense length wise twins and stacking faults, Cryst. Growth Des.28(8) (2008)3073–3076.

55. I. Chakraborty, D. Carvalho, S. N. Shirodkar, S. Lahiri, S. Bhattacharyya, R. Banerjee, U.Waghmare, P.Ayyub, Novel hexagonal poly types of silver: growth,characterization and first-principles calculations, J. Phys.: Condens. Matter 23(2011)1–12325401.

56. I. Chakraborty, S. N.Shirodkar, S.Gohil, U. V. Waghmare, P. Ayyub, Astable, quasi-2D modification of silver:optical, electronic, vibrationaland mechanical properties, and first principles calculations, J. Phys.:Condens. Matter 26 (2014) 1–10025402.

57. A. F. Marshall, S.V. Thombare, P. C. Mc Intyre, Crystallization pathway formetastable hexagonal close-packed gold in germanium nanowire catalysts, Cryst. Growth Des. 15 (2015) 3734–3739.

58. R. M. Ormerod, C. J. Baddeley, R. M. Lambert, Active alloying of Au with Pt in nanoclusters supported on a thin film of $Al_2O_3$/NiAl (10 0), Surf. Sci.259 (1–2) (1991)709–713.

59. J. B. Jia, L. Y. Cao, Z. H. Wang, Platinum-coated gold nano porous film surface: electrode position and enhanced electro catalytic activity for methanol oxidation, Langmuir 24 (11) (2008) 5932–5936.